# Impact of topography, climate and moisture sources on isotopic composition ( $\delta$ 18 O & $\delta$ D) of rivers in the Pyrenees: Implications for topographic reconstructions in small orogens

Damien Huyghe, Frédéric Mouthereau, Mathieu Sebilo, Arnaud Vacherat, Loïc Ségalen, Patricia Richard, Philippe Biron, Thierry Bariac

# Impact of topography, climate and moisture sources on isotopic composition ($\delta^{18}O$ & $\delta D$) of rivers in the Pyrenees: implications for topographic reconstructions in small orogens

Damien Huyghe[1,2], Frédéric Mouthereau[1], Mathieu Sébilo[3], Arnaud Vacherat[1], Loïc Ségalen[4], Patricia Richard[3], Philippe Biron[3], Thierry Bariac[3]

[1] Géosciences Environnement Toulouse (GET), Université Paul Sabatier Toulouse 3, 14 Avenue Edouard Belin, 31400 Toulouse, France

[2] Now at Sorbonne Universités, UPMC-Paris 06, UMR 8222, Lab. Ecogéochimie des environnements benthiques (LECOB), Observatoire Océanologique, F-66650, Banyuls-sur-mer, France

[3] Sorbonne Université UPMC Université Paris 06, Institut d'Ecologie et des Sciences de l'Environnement de Paris (IEES Paris), CNRS, Campus INRA, AgroParisTech, Bâtiment EGER, 78550 Thiverval-Grignon, France

[4] Sorbonne Universités, UPMC-Paris 06, UMR CNRS 7193, ISTeP, F-75005, Paris, France

**Abstract**

Understanding how orogenic topography controls the spatial distribution and isotopic composition of precipitation is critical for paleoaltitudinal reconstructions. Here, we determine the isotopic composition ($\delta^{18}O$ and $\delta D$) of 82 small rivers and springs from small catchments in the Pyrenees. Calculation of the deuterium excess (d-excess) parameter allows the distinction of four distinct isotopic provinces with d-excess values of between 15 and 22 ‰ in the northwest, between 7 and 14 ‰ in the central northern Pyrenees and between 3 and 11 ‰ in the northeast. The southern Pyrenees have a homogenous d-excess signature ranging from 7 to 14 ‰. Our results show significant local moisture recycling and/or rain amount effect in the northwestern Pyrenees, and control by evaporation processes during rainfall events in the southern Pyrenees and for low elevated samples of the northeast of the range. Based on the distribution of d-excess values, we estimate contrasting isotope lapse rates of -2.9/-21.4 ‰/km ($\delta^{18}O/\delta D$) in the northwest, -2.7/-21.4 ‰/km ($\delta^{18}O/\delta D$) in the north central and -3.7/-31.7 ‰/km ($\delta^{18}O/\delta D$) in the northeastern Pyrenees. The southern Pyrenees show distinctly higher lapse rates of -9.5/-77.5 ‰/km ($\delta^{18}O/\delta D$), indicating that in this area the altitudinal effect in not the only parameter driving isotopic composition of rivers. Despite their relatively low topographic gradient, the Pyrenees exert a direct control on the isotopic composition of river waters, especially on their northern side. The variations in isotopic composition-elevation relationships documented along the strike of the range are interpreted to reflect an increasing continentality effect driven by wind trajectories parallel to the range, and mixing with Mediterranean air masses. Despite these effects, the measurable orographic effect on precipitation in the Pyrenees proves that the isotopic composition approach for reconstructing past topography is applicable to low-elevation orogens.

Keywords: stable isotopes; orographic effect; paleoaltimetry; meteoric water; western Europe; climate

## 1. Introduction

Topography of continents is the expression of the coupling processes between geodynamics that govern exhumation, loading and unloading of the continental crust and earth surface processes (Mulch et al., 2016). These processes control ways in which sediments are stored and transported from mountainous areas to sink domains (e.g. Allen, 2008). The elevation of mountain ranges exerts a direct control on atmospheric circulation and thus on precipitation and climate, and has strong implications on topics as broad as geodynamics, tectonics, sedimentology, paleoclimatology or paleontology (Mulch, 2016). Documenting the evolution of Earth's surface elevation is a critical question for understanding the tectonic evolution of collisional domains, and to investigate tectonics vs climate interactions and their relative influence on erosion and sedimentation (Rowley and Garzione, 2007).

Paleoaltitudes have successfully been reconstructed for highly elevated domains like the Andean Plateau (e.g. Garzione et al., 2014) or the Himalaya and Tibetan Plateau (Caves et al., 2015; Gébelin et al., 2013) and less elevated mountains ranges like the Sierra Nevada (Mulch et al, 2016), the Alps (Campani et al., 2012) and the Pyrenees (Huyghe et al., 2012a). The fundamental principle lies in the fact that both the isotopic composition in oxygen ($\delta^{18}O$) and hydrogen ($\delta D$) in rain decreases with elevation. This first-order relationship reflects a simple Rayleigh distillation behaviour in which rainfall is increasingly depleted in the heavy isotopes ($^{18}O$ and D) with elevation (Dansgaard, 1964; Gonfiantini et al., 2001; Rowley, 2007). The rate at which this decrease occurs is measured on modern water (i.e., the isotopic lapse rate) and can then be converted to paleoelevation fluctuations as variations of the isotopic signature of minerals formed from meteoric water can be related, in principle, to a combination of climatic and elevation changes. (e.g., Rowley et al., 2001).

However, limitations have to be considered when interpreting the isotopic composition of minerals as a measure of paleoaltimetry. In particular, topography may modify the pattern of atmospheric circulation, leading to the isolation of two geographically distinct climatic provinces characterized by specific isotopic fractionation that may cause changes in the $\delta^{18}O$ composition (Ehlers and Poulsen, 2009; Insel et al., 2012). In the case of a dominant orographic effect, the windward side of the orogen experiences wet conditions, with the precipitation of moist air masses that record a typical Rayleigh distillation behaviour. On the contrary, the leeward side of the orogen is frequently characterized by the advance of dry air resulting in a local rain shadow. Due to aridity, the surface moisture is recycled to the atmosphere and suffers isotopic fractionation. Thus, precipitation related to this source of moisture does not directly conform to Rayleigh distillation processes. Reliable paleotopographic investigations are then only possible on the windward side of the range (Schemmel et al., 2013; Bershaw et al., 2016).

Modern isotopic lapse rates have been well documented from rain or river waters monitored for highly elevated mountain ranges like the Andes (Gonfiantini et al., 2001; Bershaw et al., 2016), the Sierra Nevada (Ingraham and Taylor, 1991), the Tibetan Plateau and Himalaya (Garzione et al., 2000; Chen et al., 2008; Caves et al., 2015), the Anatolian Plateau (Schemmel et al., 2013) or the Alps (Longinelli and Selmo, 2003). These studies yielded mean isotopic lapse rates of ~ -2.8 ‰/km and ~ -22 ‰/km for $\delta^{18}O$ and $\delta D$ respectively. Local deviations from these empirical relationships have been observed, and interpreted to reflect continentality or latitudinal effects (Winnick et al., 2014; Caves et al., 2015). Whether low-elevated orogens also produce measurable orographic effect on precipitation or are high enough to cause the isolation of two distinct isotopic provinces is unclear. For example, in the case of the Alps, the isotopic lapse rate is ~ -2 ‰ / km for both the northern side in Switzerland and for the southern side in Italy (Longinelli and Selmo, 2003). This result is found independently of a shift of ~ 3‰ in $\delta^{18}O$ values observed between the two sides caused by the different moisture sources. Thus, even if the isotopic lapse rates are nearly the same on the windward side of most mountain ranges all around the world, the absolute isotopic values may vary for a given elevation. Moreover, tracking isotopes in precipitation via global circulation models suggests that temporal modifications in air mass composition due to climatic and topographic variations can modify the local isotopic lapse rate and the resulting isotope-in-precipitation patterns at high elevation (Ehlers and Poulsen, 2009). Due to these uncertainties it is first required to document the local modern isotopic lapse rate from which assumptions can be formulated regarding a possible orographic effect on precipitation.

Here we focus on the Pyrenees, a small collisional orogen. Its size is beneficial to isotopic studies as a reliable and geographically extensive sampling across the range can be performed. Past elevations changes in the Pyrenees have been investigated using isotopic measurements on Eocene marine molluscs (Huyghe et al., 2012a) and Neogene pollen floras (Suc and Fauquette, 2012), proving the great potential of these techniques for yielding paleoelevation reconstructions in the Pyrenees. However, none of these studies have focused on the modern isotope vs elevation relationships in this range, which is crucial to determine if low-elevated mountain ranges are capable of exerting a control on the isotopic composition of precipitation, as was argued by previous studies. Moreover, working on the Pyrenees introduces specific problematic aspects compared to many other mountain ranges like the Andes, the Himalaya or the Sierra Nevada, because the main source of moisture, which is located in the Atlantic Ocean, is only slightly oblique to the topography (Fig. 1A).

## 2. Geological setting

The Pyrenees are a doubly vergent collisional orogen resulting from collision between the Iberian and European plates from the Late Cretaceous to the Middle Miocene (Muñoz, 1992; Vergés et al., 2002). This range presents the advantage of having been well documented for several aspects, including tectonic (e.g. Muñoz, 1992; Vergés et al., 2002; Mouthereau et al., 2014), geomorphologic (Babault et al., 2005; Gunnell et al., 2008) or sedimentologic and exhumational (Christophoul et al., 2003; Huyghe et al., 2012b; Vacherat et al., 2017) evolution. These previous studies show that shortening and exhumation were fastest during the Eocene and Oligocene times (Sinclair et al., 2005). This led to an increase in both erosion rates in the growing mountain range and detrital sedimentation rates in the adjacent foreland basins (Huyghe et al., 2009, 2012b; Filleaudeau et al., 2012). The paleogeographic and sedimentologic histories of the two foreland basins are different during the collision (Vacherat et al., 2017). The northern Pyrenees has always remained connected to the Atlantic Ocean and to the Mediterranean Sea since the Oligocene. On the contrary, the South-Pyrenean foreland basin was open towards the Atlantic Ocean only up until the Late Eocene. The uplift of the Cantabrian mountain belt led to the closure of the basin connection with the Atlantic, which became internally-drained. In the Late Miocene, the basin reconnected to the Mediterranean Sea (Garcia-Castellanos et al., 2003; Vacherat et al., 2017). Due to the endorheic phase, the South-Pyrenean foreland accumulated sediments sourced from the growing topography, which ultimately led to a reduction of the slope of the rivers and their erosive effectiveness (Babault et al., 2005).

## 3. Modern topography and climate

The Pyrenean range is nearly 600 km long east-west and is maximum 150 km wide in a north-south direction, with a maximum elevation of 3404 m at the Pic d'Aneto (Fig. 1A). Smaller mountainous reliefs occur around the Pyrenean domain and also contribute to the regional pattern of atmospheric circulation and precipitation. In Spain, these are from west to east, the Cantabrian Range, which corresponds to the western prolongation of the Pyrenees on the northern coast of the Iberian Peninsula; the Iberian Range, corresponding to the southern border of the Ebro Basin, which was inverted between the Late Cretaceous and the Miocene; and the Catalan Coastal Range (Fig. 1A). In France, the Corbières and the Montagne Noire correspond to small massifs in the northeastern Pyrenees. The southern and the northern Pyrenean domains exhibit a contrasting topographic pattern in that the northern side exhibits a steeper mean slope with highly incised valleys, contrary to the southern flank that is wider with a more gentle mean slope. These differences mainly reflect the variable long-term response of river incision to base level changes. The northern Pyrenean rivers are connected to the Atlantic Ocean and the Mediterranean Sea, whereas the Ebro drainage system cuts across a former endorheic basin.

The precipitation pattern around the Pyrenees is primarily controlled by the distribution of the topography, with the highest mean annual precipitation (MAP) observed at the highest elevations (Fig. 2A). For the low elevation areas bordering the range, the highest MAP is observed along the Atlantic coast in the northwestern Pyrenees (1450 mm/yr in Biarritz) (Fig. 2C). Over the northern Pyrenean piedmont, precipitation strongly decreases eastwards until the Lannemezan Plateau (1047 mm/yr at Campistrous). Eastwards, in the northeastern Pyrenees, precipitation decreases and reaches 557 mm/yr along the Mediterranean coast, in the city of Perpignan. In the southern Pyrenees, MAP is maximum along the Atlantic coast (1740 mm/yr in San Sebastian), then gradually decrease to the east (720 mm/yr in Pamplona and 370 mm/yr in Huesca). MAP increases slightly in the southeastern Pyrenees, with 685 mm/yr in Girona along the Mediterranean coast. MAP is thus lower in the southern Pyrenean piedmont than in the northern one.

The main source of moisture over the Pyrenees is the northern Atlantic and related to the North Atlantic Oscillations (Fons, 1979; Lambs et al., 2003; Araguas-Araguas and Diaz Teijeiro, 2005). However, moisture can also be sourced from the western Mediterranean Sea and northern Europe (Lambs et al., 2003; Araguas-Araguas and Diaz Teijeiro, 2005). To accurately determine the origin of the moisture over the Pyrenees, we used the HYbrid Single-Particle Lagrangian Integrated Trajectory Model (HYSPLIT) (Stein et al., 2015) to track air parcel trajectories around the main topography (Fig. 1B to 1F). We selected five locations, three on the northern side of the range and two in the southern side, so as to cover the entire analysed domain for isotopic composition. We computed 72h back trajectories every 12h for each location, for the months of April and May 2013. These are the rainiest of the year, before the dry season, during which we sampled river waters. In this analysis, we only report trajectories that provided precipitation over the Pyrenees, representing a maximum of 471 trajectories in the northwest to a minimum of 156 to the southeast of the range. These data clearly indicate that the Atlantic Ocean is the main source of moisture for the rain sourcing the Pyrenean rivers, and that Mediterranean and northern European sources are limited in comparison.

Mean annual temperatures (MAT) are correlated to the distribution of the precipitation, with an overall correlation with elevation. At low elevation, we observe a general warming trend from west to east to the north and relatively homogenous warm MAT in the southern Pyrenees (Fig. 2B). Temperature seasonality is higher in the southern and in the northeastern Pyrenees (~ 16-17 °C) than in the northwestern and central northern Pyrenees

(12-14 °C) (Fig. 2C). This likely highlights the diversity of local climatology across this range, ranging from oceanic to sub-continental to Mediterranean from west to east.

Oxygen isotope values are available from three GNIP (Global Network of Isotopes in Precipitation, http://www.iaea.org/water) stations at low elevation in the northern Pyrenees. One station located close to the Atlantic coastline (Dax) documents weighted mean annual $\delta^{18}O$ of -5.4‰ and weighted mean annual δD of -31.9‰. A second one from the central Pyrenees, at the foot of the main topographic relief at the head of the Lannemezan alluvial fan (Campistrous), yields mean annual $\delta^{18}O$ and δD of -7.5‰ and – 46.3‰ respectively. Another one in Toulouse yields $\delta^{18}O$ of -6.3‰ and δD of -38.8‰ (Fig. 1, Supplementary data 1). GNIP stations from northern Spain are located relatively far from the Pyrenees, in the South-Pyrenean foreland (Zaragoza, $\delta^{18}O$ = -5.7‰ and δD = -40.1‰), in Barcelona ($\delta^{18}O$ = -4.74‰ and δD = -26.8‰) on the Mediterranean coast and in Girona ($\delta^{18}O$ = -5.2‰ and δD = -34.4‰). Correlation between isotopic values and climatic parameters at each station indicates that $\delta^{18}O$ and δD are mostly correlated with seasonal temperature variations rather than with the amount of precipitation (Supplementary data 1).

## 4. Material and method

Several sampling strategies are possible to document a topographic effect on the isotopic composition of precipitation and rivers. The most obvious way is a direct monitoring of rain at different locations and at various elevations. However, this approach presents some logistical limitations because it requires a large network of stations all around the range, with regular and synchronous samplings.

Isotopes vs. elevation investigations are therefore traditionally performed on rivers and streams at different elevations (Schemmel et al., 2013; Bershaw et al., 2016; Li and Garzione, 2016). This approach presents many advantages, because it allows a wide and representative sampling all over the mountain range. Moreover, during the dry season, groundwaters dominates the budget of small rivers and streams that correspond to a mix of the yearly rain, representing an annual mean of the isotopic composition of rain (Ingraham and Taylor, 1991; Schemmel et al., 2013). This allows avoiding the influence of transient climatic events on the isotopic composition of rivers, during which isotope/temperature data might not be correlated (Celle et al., 2000). The counterpart is that river and stream waters correspond to a mix of all rainfalls precipitated in the catchment above the sampling point and it is important to study small ones to avoid uncertainties related to the integration of a large elevation range (Poage and Chamberlain, 2001). We avoid sampling spring waters because of the lack of accuracy regarding the elevation at which rain effectively fell above the resurgence (Schemmel et al., 2013).

We have sampled 82 rivers and streams in the whole Pyrenees (Fig. 1A). They are draining ten main valleys in France, Spain and Andorra. More samples from the northern Pyrenees were collected due to the asymmetric distribution of precipitation and aridity between the two sides (Fig. 2). Thus, from west to east, we have sampled five main transects across the range. First, in the Basque Country, profile A-C begins near sea level south of Biarritz and crosses the divide at the Ronceveaux pass (B). It continues to the southwest and ends near the city of Pamplona (C). The second profile (D-F) is continuous from Pau to Huesca with a maximum elevation (~ 1750 m) at the Pourtalet pass (E). Stream and rivers were sampled in tributaries along the Ossau valley in France and along the Rio Gallego and Rio Isuela valleys in Spain. Six samples come from Navarre, between profiles B-C and E-F and are not integrated in any profile. The third profile (G-I) begins in France on the slope of the Lannemezan alluvial fan and continues to the mains reliefs though the Neste d'Aure valley up to its source (H). The profile continues to the south along the Rio Noguera Ribagorçana and Noguera Pallaresa valleys (H'-I) in the Tremp Basin. Only four points could be sampled in this area due to the elevated aridity. The fourth profile (J-L) begins to the south of Toulouse, with samples have been collected in tributaries along the Ariège valley up to the highest samples from Andorra (K; ~ 2100 m). The profile continues through the Cerdanya Basin and the Sierra de Cadi to the south. The last profile (M-N) is oriented W-E and begins at the top of the Têt valley. Samples come from small tributaries of the Têt River and finishes south of Perpignan in the Roussillon Plain, near sea level.

Water was sampled during the dry season, from July to September, in summers 2013 to 2015, at least one week after the last rain, to minimize the effect of recent climatic events. For each sample, 20 ml of water were collected and conditioned at low temperature to avoid fractionation effects caused by evaporation.

Analyses were performed at the Institut d'Ecologie et des Sciences de l'Environnement de Paris at Grignon. $\delta^{18}O$ analyses were performed by $CO_2$-$H_2O$ equilibration (Epstein and Mayeda, 1953) using isotope ratio mass spectrometer coupled to an Aquaprep (Isoprime coupled to a Gilson X222, Micromass; standard error: 0.15 ‰). $\delta D$ measurements were produced by pyrolysis of the water molecule on a chrome reactor, with continuous flow of ultra-pure helium using an isotope mass spectrometer PyrOH (Isoprime coupled to an elemental analyzer EuroVector, Micromass; standard error: 0.8 ‰) (Morrison et al., 2001). Oxygen and hydrogen isotopic measurements were expressed in "δ" notation.

## 5. Results

Results are summarized in Fig. 3, in which the spatial distribution of $\delta^{18}O$ and $\delta D$ of streams and rivers around the Pyrenees is presented. The dependence on elevation is the same for the two isotopic ratios. The highest values are observed at low elevation whereas the ratios drop to negative values at high elevation. $\delta^{18}O$ ranges from -5.5 ‰ to -12.1 ‰ in the northern Pyrenees and from -6.5 ‰ to -11.1 ‰ in the southern Pyrenees. $\delta D$ values range from -27.7 ‰ to -84.1 ‰ in the north and from -42.8 ‰ to -76.9 ‰ in the south. Figures 3B and 3D show the $\delta^{18}O$ and $\delta D$ isotopic composition of river waters projected onto a topographic profile perpendicular to the central Pyrenees. Despite the apparent scattering of isotopic values with elevation, reflecting the variability of $\delta^{18}O$ and $\delta D$ along the strike of the range, the figure shows that the northern side of the Pyrenees displays an isotope vs. elevation relationship that is not so clearly seen in the southern Pyrenees, especially at low elevation (Fig. 3B and 3D).

Plotting our $\delta^{18}O$ and $\delta D$ data for each area, valley by valley, the dependence of isotopic ratios relative to elevation appears more clearly (Fig. 4 and 5). To the west (profile A-C), near sea-level values for the French Basque Country range between -5.7 and -6.3‰ for $\delta^{18}O$ and -27.7 and -31.9‰ for $\delta D$. Dependence on elevation is well documented for the French side, with a decrease of the isotopic ratios above the Ronceveaux pass at 1230 m (-9.3‰ for the $\delta^{18}O$ and -53.1‰ for the $\delta D$). In contrast, $\delta^{18}O$ and $\delta D$ values are relatively constant in the southern side (B-C) and even decrease with elevation. On profile D-F, minimum values are reached at the Pourtalet pass (-11 ‰ and -75.4 ‰ for $\delta^{18}O$ and $\delta D$ respectively). In this profile, we observe a decrease of $\delta^{18}O$ and $\delta D$ with elevation on both sides of the range. A local decrease of isotopic ratios on top of the Sierra Exteriores is resolved in the southern Pyrenees. On profile G-H, a strong decrease of isotopic composition is measured from 220-280 m near the Lannemezan alluvial fan (~ -7 ‰ for $\delta^{18}O$ and ~ -65 ‰ for $\delta D$) to elevation of ~ 1800 m at Piau Engaly (-12.1 ‰ the $\delta^{18}O$ and -83.5 ‰ for $\delta D$). The scattering of isotopic compositions of waters is more significant on profile H-I, so correlations between elevation and $\delta^{18}O$ and $\delta D$ appear less clear. On profile J-L, the highest $\delta^{18}O$ (-7.5 ‰) and $\delta D$ (-49 ‰) are observed at the lowest elevation (~ 300 m) for the northern Pyrenees and the most negative $\delta^{18}O$ (-11.9 ‰) and $\delta D$ (-82.4 ‰) at 1800-2300 m in Andorra. Values increase to the south in the Cerdanya Basin and through the Sierra de Cadi and the northern Ebro Basin to reach -6.8 ‰ ($\delta^{18}O$) and -42.8 ‰ ($\delta D$) at 1100 m. Isotopic compositions along the Têt valley (M-N profile) are well correlated with elevation from 1725 m (-11.7 ‰ for $\delta^{18}O$ and -85.4 ‰ for $\delta D$) to the coast (max. $\delta^{18}O$ = -5.5 ‰ and $\delta D$ = -38.8 ‰). Thus, the near sea-level samples of the two northern terminations of the range have similar $\delta^{18}O$ values, whereas $\delta D$ is slightly more negative to the east. The decrease in isotopic composition with elevation is obvious on the whole northern side of the range and is less clear in some profiles in the southern Pyrenees.

## 6. Discussion

### *6.1. Significance of the spatial distribution of the isotopic values*

To determine the moisture origin and to identify a possible recycling effect caused by the evaporation of a surface water reservoir or during rainfall, we have calculated the deuterium excess parameter (d) (Daansgard, 1964; Merlivat and Jouzel, 1979) (Fig. 6). This parameter links the $\delta^{18}O$ and $\delta D$ of water ($d = \delta D - 8 \times \delta^{18}O$). It can be considered as an index of deviation from the Global Meteoric Water Line (GMWL), which is characterized by a d-excess value of 10 ‰. d-excess is a parameter sensitive to the initial conditions during evaporation from the ocean surface and is therefore a function of both temperature and relative humidity at the oceanic source, as well as the speed of the wind and resistivity to liquid – vapour transfer via a kinetic isotopic fractionation (Merlivat and Jouzel, 1979; Froehlich et al., 2001). It is also a function of the conditions during the transport of moist air and/or mixing of different air masses before moisture is condensed to form rainfall (Froehlich et al., 2001). The general pattern is that d-excess in precipitation increases in response to enhanced moisture recycling as a result of increased evaporate content. On the contrary, d-excess is low when water is lost from air masses or rainfall due to evaporation (Froehlich et al., 2001).

In the Pyrenees, the calculation of d-excess allows the identification of four different water populations, characterized by distinct d-excess values (Fig. 6). First, in the northwestern Pyrenees (profiles A-B and D-E, Fig. 1) d-excess is high and ranges from 15 ‰ to 22 ‰. The central northern Pyrenees (G-H and J-K, Fig. 1) have intermediate d-excess values, between 7 and 14 ‰, whereas French Catalonia (M-N) have the lowest d-excess values, ranging from 3 ‰ to 11 ‰. In Spain, d-excess values are more homogenous and range from 7 ‰ to 14 ‰.

Considering back trajectory analysis, the mains sources of moisture in the Pyrenees are the northern Atlantic Ocean and, at a lower proportion the Mediterranean Sea (Fig. 1). A value of d ~ 10 ‰ is generally considered for moisture coming from the Atlantic Ocean to southwestern Europe (Lambs et al., 2003) whereas the western Mediterranean Sea has a rather higher d-excess (~ 14 ‰) due to its closed configuration (Celle et al., 2000). French GNIP stations show higher mean annual weighted d-excess values than their Atlantic Ocean source and lower than the western Mediterranean one, evolving from 11.3 ‰ at Dax to 13.4 ‰ at Campistrous and to 11.8 ‰ at Toulouse (Supplementary data 1). River waters sampled at low elevation also have high d-excess (~ 18 to 19 ‰) near the French Atlantic coast (A-B) and in the Ossau Valley (D-E), and decrease in the central Pyrenees to 10 – 13 ‰ (G-H and J-K). This pattern could reflect a possible mixing between Atlantic and Mediterranean moisture, but the latter is supposed to have an influence only on the eastern coastline (Lambs et al., 2003). HYSPLIT back trajectory analysis confirms that the north Atlantic Ocean is the main source of moisture in the northwestern Pyrenees. Then, the high d-excess values of rain and rivers of the northwestern Pyrenees are likely the expression of local surface water recycling (Froehlich et al., 2001). The northwestern Pyrenees are also the location where MAP is the highest at low elevation, so that these high d-excess values could also reflect the influence of the amount effect (Lee and Fung, 2008; Botsyun et al., 2016).

It is worth noting that d-excess may show strong seasonal variations, such as seen at the GNIP station of Dax between winter (d = ~15 ‰) and summer (d = ~3 ‰) due to colder and less humid air masses during winter in the north Atlantic (Gonfiantini et al., 2001). Yet, rainfall amounts and air temperatures exhibit strong seasonal variations, with maximal precipitation and minimal temperatures being observed during winter and spring. It is likely that the isotopic composition of the weighted mean annual values of rain at the three GNIP stations and those of the Pyrenean rivers represent winter and spring values in majority, due to this seasonally contrasted amount of rain and temperatures. We observe, however, that monthly isotopic compositions of rain always present a better correlation with temperature than precipitation values (Supplementary data 1).

Isotopic values of rivers at low elevation in northwestern and central northern Pyrenees are also lower compared to values at the GNIP stations, with a difference of 0.5 to 1.5 ‰ and 1.5 to 12 ‰ for $\delta^{18}O$ and $\delta D$ respectively (Fig. 6). The difference could reflect isotopic fractionation in rain feeding rivers versus rain directly sampled at the stations. However, it is important to determine what the water sampled in the Pyrenean rivers do represent compared to rain. In the northwestern and central northern Pyrenees, the isotopic composition of rain exhibits strong seasonal variations at the GNIP stations of Dax (from -2.3 ‰ to -6.8 ‰ for $\delta^{18}O$ and -14.5 ‰ to -45.8 ‰ for $\delta D$), Campistrous (from -3.2 ‰ to -9.8 ‰

for $\delta^{18}O$ and -15.2 ‰ to -66 ‰ for δD) and Toulouse (from -4.5 ‰ to -10.2 ‰ for $\delta^{18}O$ and -24.8 ‰ to -71.8 ‰ for δD), with the most negative values recorded during winter (Supplementary data 1). The amount of precipitation is also governed by seasonal cyclicities and is the highest from October to May (Fig. 2).

On Fig. 7 we report the weighted mean and winter (from October to May) isotopic values of rain at the GNIP stations of Dax, Campistrous and Toulouse and the isotopic composition of rivers at low elevation located in the same area as these GNIP stations. Winter isotopic values at GNIP stations shift to more negative values than the mean annual values (Fig. 7). We also observe that GNIP winter and spring values are close to river samples at the same elevation as the Campistrous GNIP Station. $\delta^{18}O$ and δD of rain remain slightly higher at Toulouse for the low elevation samples from the Ariège valley, but these last ones were sampled at mean elevation ~200 m higher than the Toulouse station. If we consider a mean elevation effect of –0.28 ‰/100 m for $\delta^{18}O$ and –2.2 ‰/100 m for δD, as observed in many other orogens (Rowley and Garzione, 2007), the weighted mean winter isotopic values of rain at Toulouse fit with the low elevation samples of the Ariège valley (Fig. 7). Concerning the French Basque Country (A-B), winter values at Dax are closer for $\delta^{18}O$, but remain different for δD. This difference highlights that our river samples rather reflect winter and spring isotopic values of rain than a mean of the annual values. It also illustrates that the effect of moisture recycling is limited to the border of the Pyrenean range and that it is attenuated away from the mains reliefs like at Dax.

In French Catalonia (profile M-N), d-excess values at low elevation are very low (d = ~ 3-5 ‰). Back trajectory analysis reveals that rainfalls in the area come from the northern Atlantic Ocean and the western Mediterranean Sea. d-excess values in this area are significantly lower than thoses of the northern Atlantic (d = 10 ‰) and the western Mediterranean Sea (d = 14 ‰). This difference reflects the influence of evaporation processes on rain that source the eastern Pyrenean rivers (Froehlich et al., 2001). However, in this part of the range, low d-excess values are only observed at low elevation, where the highest temperature and lower precipitation are recorded in the area (Fig. 2). d-excess values are higher in the upper part of the Têt valley (profile M-N), where MAT are lower and precipitation increases (Fig. 6). This suggests that northeastern Pyrenean river-waters sampled at low elevation probably experienced evaporation compared to rain precipitated at higher elevation, and are not fully representative of the initial isotopic compositions of rain. Indeed, these samples come from small rivers with very reduced flow. We will thus not consider these values further.

In the southern Pyrenees, d-excess is more homogenous and ranges from 7 to 14 ‰. We do not observe significant variations in the southwestern to southeastern Pyrenees that could suggest the possible influence of different moisture sources, as the origin of the moisture remains nearly the same (i.e. Atlantic Ocean and Mediterranean Sea) in the whole southern Pyrenees (Fig. 1E and 1F). Moreover, d-excess is variable even for samples at low elevation. River samples at low elevation are located too far from the Spanish GNIP stations to make a reliable comparison like in France, but we can see great discrepancies in first approach.

### *6.2. Meteoric water lines*

We have calculated the Local Meteoric Water Lines (LMWL), by plotting δD against $\delta^{18}O$ values in Fig. 8. We see that all Pyrenean values exhibit a relatively good overall correlation, with a small shift above the Global Meteoric Water Line (GMWL), but a similar slope (~ 8) (Fig. 8A). We also present a separate plot four distinct isotopic provinces based on d-excess values (Fig. 8B). Outliers reveal the existence of four isotopic provinces that exhibit distinct isotopic characteristics, and that give three LMWL for the northern Pyrenees and one for the south:

$$\text{Northwestern Pyrenees: } \delta D = 7.67\ \delta^{18}O + 15.47 \quad (1)$$

$$\text{Central northern Pyrenees: } \delta D = 7.79\ \delta^{18}O + 9.82 \quad (2)$$

$$\text{Northeastern Pyrenees: } \delta D = 8.15\ \delta^{18}O + 10.12 \quad (3)$$

The northwestern Pyrenees present the most distinct values (eq. 1; Fig. 8B). The correlation line is the most shifted, but the slope is close to the GMWL. The central northern Pyrenees follow the same tendency, with a shift to values closer to the GMWL (eq. 2). After the removal of values at low elevation with very low d-excess, the northeastern Pyrenees exhibit a relationship that is very close to the GMWL (eq. 3). It is also close to the relationship determined by Celle et al. (2000) for the station of Avignon in southern France.

We also plotted isotopic compositions of rivers against MAP and MAT, extracted for each sampling area from the data of Hijmans et al. (2005) (Fig. 8C to 8F). We observe that the isotopic compositions of the northwestern Pyrenean rivers are poorly correlated with MAP ($R^2$ of 0.06 and 0.05 for $\delta^{18}O$ and $\delta D$ respectively), contrary to MAT ($R^2$ of 0.8 for $\delta^{18}O$ and $\delta D$). On the contrary, central northern and northeastern Pyrenees exhibit good correlations with both MAP and MAT ($R^2$ comprised between 0.7 and 0.85).

The good agreement of these three LMWL with the GMWL shows that river waters reflect regional precipitation and that the evaporation effect is small. We conclude that the isotopic composition of rain and rivers in the northern Pyrenees results principally from temperature variations and thus from the altitudinal effect. This suggests that the Pyrenees are high enough to exert an orographic effect on the isotopic composition of rain and rivers.

The Spanish Pyrenees show the lowest slope that cuts the GMWL:

$$\text{Southern Pyrenees: } \delta D = 7.26\ \delta^{18}O + 3.89 \qquad (4)$$

The slope measured for the southern Pyrenean LMWL is the lowest of the four isotopic provinces around the Pyrenees, but it remains close to the GMWL. This low slope is probably due to the evaporation of moisture during rain events as a consequence of higher MAT and lower MAP on the southern side of the range compared to the northern side (Celle et al., 2001). In this area, isotopic compositions of rivers show weak correlations with both MAP and MAT (Fig. 8C to 8F).

The deviation from the GMWL remains limited however compared to highly elevated mountain ranges where the slope of the LMWL in the true leeward side is > 6, like in the Andes or the Central Anatolian Plateau (Gonfiantini et al., 2001; Schemmel et al., 2013). Thus, the southern Pyrenees cannot be considered as a true leeward side influenced by a real rain shadow effect.

We can define several processes from these four LMWL. The first orographic precipitation from the northern Atlantic source falls over the whole northwestern Pyrenees, and has relatively homogenous characteristics at least 150-200 km inland. Due to the continentality effect, as moisture is translated to the central Pyrenees, the isotopic composition of rain water follows a distinct LWML with a slope close to the GMWL that is similar to the northwestern Pyrenees. This evolution can be considered as the result of the continentality effect, as littoral domains receive rainwater corresponding to the firsts steps of moisture condensation with enriched isotopic values. A similar slope between the two isotopic provinces shows that clouds migrate inland without suffering significant evaporation or water recycling. Back trajectory analysis indicates that the influence of the western Mediterranean Sea is proportionally more important in the northeastern Pyrenees (profile M-N) than in the northwestern and north central Pyrenees and represents a more equilibrated mix of the Atlantic and Mediterranean moisture sources (Fig. 1D). We note however that the contintentality effect is greater on the Atlantic source, which is still important for the origin of the rain arriving in the northeastern Pyrenees. The southern Pyrenees constitute an isotopically more isolated area compared to the north, where precipitation is lower and moisture more recycled to the atmosphere during rainfall events.

### *6.3. Isotopic lapse rate*

Considering that elevation to first order drives the isotopic composition of rain in the French Pyrenees, we have calculated isotopic lapse rates for $\delta^{18}O$ and $\delta D$ for the four studied isotopic provinces (Fig. 9). Modern isotopic lapse rates constitute a cornerstone for paleoelevation studies. As we sampled rivers and not directly rain, we need to apply a correction accounting for the mean basin hypsometry that corresponds to the average elevation of the watershed upstream from the sampling area (Poage and Chamberlain, 2001). This is why we have sampled river waters as high as possible in the watersheds. At the scale of the Pyrenees, we have calculated a mean difference of ~ 180 m between the sampling elevation of springs and rivers and the mean elevation of the corresponding watershed.

Results indicate that isotopic lapse rates differ for the four studied areas. The lowest lapse rates are measured in the northwestern Pyrenees (-2.6 and -21.4 ‰/km for $\delta^{18}O$ and $\delta D$

respectively). The central northern Pyrenees exhibit slightly higher isotopic lapse rates, increasing strongly in the northeastern Pyrenees and passing from -2.8 to -3.8 ‰/km for $\delta^{18}O$ and -21.4 ‰/km to -31.7 ‰/km for δD. The isotopic values obtained in the French Pyrenees are in good agreement with the global means of isotopic lapse rates recovered for the windward sides of the main orogens, which are -2.8 ‰/km and -22 ‰/km for $\delta^{18}O$ and δD respectively (Rowley and Garzione, 2007). Lapse rates are much higher on the Spanish side of the Pyrenees (–9.5 ‰/km and –77.5 ‰/km), with a great scattering of isotopic data and a very low coefficient of correlation. This result confirms that the elevation effect is not the dominating factor on the isotopic composition of rain and rivers in that side of the range. Therefore, reliable paleoelevation quantifications are difficult to obtain on the southern flank of the Pyrenees.

We have also reported on Fig. 9 the mean annual and winter weighted isotopic values of the GNIP stations. It appears that the Spanish GNIP stations are at odds with the lapse rate from river samples on the southern side of the range. Concerning the French stations, mean annual GNIP values are enriched compared to the river samples, except for deuterium in the French Basque-Country. However, the mean weighted winter values are shifted to more negative values, which better fits with the isotopic compositions of rivers. This finding confirms that our samples reflect the mean of precipitation during winter and spring.

## 7. Implications for paleotopographic reconstructions

Figure 10 presents a comparison between the Pyrenees and the other main mountain ranges where $\delta^{18}O$ vs elevation relationships have been investigated (Fig. 10). The figure demonstrates that the northern side of the Pyrenees shows an isotopic lapse rate close to -2.8

‰/km, in good agreement with other highly elevated mountain ranges of the world. Pyrenean $\delta^{18}O$ values of rivers at low elevation are close to those of the northeastern Bolivian Plateau and both the measured river and modelled precipitation of the south central Himalaya (~ -7 to -6 ‰; Garzione et al., 2000; Rowley et al., 2001). In Europe, values at low elevation from the northern Pyrenees are slightly more positive, but close to the published values from the southern Alps (Schotterer et al., 1997) and the Pontic Montains (Northern Central Anatolian Plateau; Schemmel et al., 2013).

Our results imply that, despite their relatively low elevation, the Pyrenees exhibit the classical features of highly elevated mountains ranges. First, they are characterized by a distinct northern side, where precipitation dominates compared to evaporation and where the altitudinal effect is the main parameter controlling the isotopic composition of rain and rivers. However, on the southern side, elevation is not the only parameter controlling isotopic composition of rivers. A probable control by evaporation during rainfall, or of surface moisture, appears to hinder reliable estimates of the altitudinal effect on isotopic composition of precipitation. Our study shows that the Pyrenees constitute a promising site for the investigation of paleoaltitudes, and the establishment of arid conditions on its southern flank through isotopic approaches.

However, the geographic and climatic features of the Pyrenees introduce specific biases that are important to consider for paleoaltitude investigations. In particular, the orientation of the main topography is parallel to the main wind trajectory and orthogonal to the coasts. Two main sources of moisture are reported on both sides of the range on the northern side. In addition, the effect of continentality and mixing of these distinct moisture sources is reflected along the strike of the orogen in the differences in isotopic lapse rate of ~ 1 ‰/km and ~ -10 ‰/km for $\delta^{18}O$ and $\delta D$ respectively.

## 8. Conclusion

We have demonstrated that, despite their relative low elevation and size compared to other ranges like the Andes, the Sierra Nevada or the Himalaya, the Pyrenees exert an orographic effect on precipitation and isotopic composition of rain and rivers. The two sides can be distinguished according to their climatic and isotopic signatures. To the north, precipitation dominates compared to evaporation, and the altitudinal effect is the main driver of the $\delta^{18}O$ and $\delta D$ composition of rain. To the south, precipitation is lower at low elevation. As a consequence, moisture is more recycled and the altitudinal effect and amount effects are not the only parameters controling the isotopic composition of rain. No reliable paleoaltitudinal reconstructions are therefore possible on this side of the orogen. A significant lateral isotopic gradient is documented from west to east due to a combination of the continentality effect and the influence of two moisture sources. As a consequence, local lapse rates have to be taken into account depending on the area considered along the strike of the orogen. These new results provide critical constraints for future investigations of past elevation reconstructions of small mountain ranges using stable isotopic geochemistry.

## Acknowledgements

We would like to thank Christelle Arduini, Nicolas Beaudoin and Franck Lartaud for their help on the field and Xavier Lalande for is help on Qgis. This work is a contribution to ANR PYRAMID Project. Editor Derek Vance, Svetlana Botsyun and an anonymous reviewer are thanked for their fruitful comments that improved the manuscript.

**Figure captions**

**Figure 1**: A: Location of samples analyzed in this study and GNIP Stations. Samples with white circles are the rivers at low elevation compared to the three French GNIP stations in Figure 7. HYSPLIT back trajectories analyses are presented for five areas around the Pyrenees, indicating the origin of the moisture up to 72h before its arrival. Back trajectories end points are located B: in the northwestern C: in the northern central D: in the northeastern, E: in the south central and F: in the southeastern Pyrenees respectively.

**Figure 2**: A: mean annual precipitation and B: mean annual temperature around the Pyrenees (from Hijmans et al., 2005). C: mean monthly temperature and precipitation from GNIP stations for Campistrous, Toulouse, Perpignan and Girona, from Météo France for Biarritz and from the State Meteorological Agency (AEMET) of Spain for Pamplona and Huesca.

**Figure 3**: A: $\delta^{18}O$ values of small rivers and streams sampled around the Pyrenees. B: projection of $\delta^{18}O$ values along a topographic cross section in the central Pyrenees. C: $\delta D$ values of small rivers and streams sampled around the Pyrenees. D: projection of $\delta D$ values along a topographic cross section in the central Pyrenees.

**Figure 4**: Distribution of $\delta^{18}O$ values of small rivers and streams in each valley sampled around the Pyrenees (except the Navarre area). Mean annual temperature and precipitation profiles are reported for each area (from Hijmans et al., 2005). Mean annual weighted value for the Campistrous GNIP station is reported in the Lannemezan – Aure valley profile (G-H).

**Figure 5**: Distribution of δD values of small rivers and streams in each valley sampled around the Pyrenees (except the Navarre area). Mean annual temperature and precipitation profiles are reported for each area (from Hijmans et al., 2005). Mean annual weighted value for the Campistrous GNIP station is reported in the Lannemezan – Aure valley profile (G-H).

**Figure 6**: Distribution of the deuterium excess parameter (d) for rivers and streams around the Pyrenees. The differences in d-excess values in each valley allow the identification of four main isotopic provinces around the Pyrenees: northwestern, central northern, northeastern and southern Pyrenees.

**Figure 7:** Plot of $\delta^{18}O$ vs. δD values for the French Basque-Country, Lannemezan and Ariège valley at low elevation and the mean annual and winter (October to April) weighted values of the Dax, Campistrous and Toulouse GNIP stations. IThe isotopic composition of rivers mostly reflects the isotopic composition of rain precipitate during the winter season. The Global Meteoric Water Line (GMWL) is also reported. River samples at low elevation are located in Fig. 1 for each sector.

**Figure 8**: Meteoric water lines (δD vs $\delta^{18}O$ relationships) of all water samples from the whole Pyrenees (A) and separately for each isotopic province in the northern and southern Pyrenees (B) as done using deuterium excess values. The Global Meteoric Water Line (GMWL) is also reported. C and D: plot of $\delta^{18}O$ and δD values against mean annual precipitation values at the sampling point, extracted from Fig. 2A. E and F: plot of $\delta^{18}O$ and δD values against mean annual temperature at the sampling point, extracted from Fig. 2B.

**Figure 9**: Isotopic lapse rates for the four isotopic provinces. Elevation corresponds to the mean elevation in the watershed upstream of the sampling site. Mean annual and winter (October to May) values of the French GNIP stations are also reported.

**Figure 10**: Modern $\delta^{18}O$ isotopic lapse rates from rain or surface water measurements for the main studied mountain ranges of the world illustrating the isotopic variability according to the initial isotopic composition of the moisture source. The calculated lapse rates for the French Pyrenees are also reported, showing good correspondance with the most elevated mountain ranges.

**Supplementary data 1:** Climatic and isotopic data of the GNIP stations around the Pyrenees in France and Spain (IAEA/WMO, 2017). Data for Toulouse are from Lamb et al., 2013. Winter values are calculated from monthly data of each station from October to May, weighted from the amount of precipitation.

**Supplementary data 2:** Isotopic composition and location of the river-water sampled in this study.

## References:

Allen, P., 2008. From landscapes into geological history. Nature 451, 274-276.

Araguas-Araguas, L.J., Diaz Teijeiro, M.F., 2005. Isotope composition of precipitation and water vapour in the Iberian Peninsula. In: Isotopic composition of precipitation in the Mediterranean Basin in relation to air circulation patterns and climate. International Atomic Energy Agency-Isotopic composition of precipitation in the Mediterranean Basin in relation to air circulation patterns and climate. International Atomic Energy Agency, 173-190.

Babault, J., Van Den Driessche, J., Bonnet, S., Castelltort, S., Crave, A., 2005. Origin of the highly elevated Pyrenean peneplain. Tectonics 24, TC2010.

Bershaw, J., Saylor, J.E., Garzione, C.N., Leier, A., Sundell, K.E., 2016. Stable isotope variations ($\delta^{18}O$ and $\delta D$) in modern waters across the Andean Plateau. Geochimica et Cosmochimica Acta 194, 310-324.

Botsyun, S., Sepulchre, P., Risi, C., Donnadieu, Y., 2016. Impacts of Tibetan Plateau uplift on atmospheric dynamics and associated precipitation $\delta^{18}O$. Climate of the Past 12(6), 1401-1420.

Campani, M., Mulch, A., Kempf, O., Schlunegger, F., Mancktelow, N., 2012. Miocene paleotopography of the Central Alps. Earth and Planetary Science Letters 337-338, 174-185.

Caves, J., Winnick, M.J., Graham, S.A., Sjostrom, D.J., Mulch, A., Chamberlain, C.P., 2015. Roel of the westerlies in Central Asia climate over the Cenozoic. Earth and Planetary Science Letters 428, 33-43.

Celle, H., Daniel, M., Mudry, J., Blavoux, B., 2000. Signal pluie et traçage par les isotopes stables en Méditerranée occidentale. Exemple de la région avignonnaise (Sud-Est de la France). Comptes Rendus de l'Académie des Sciences-Series IIA-Earth and Planetary Science 331(10), 647-650.

Celle-Jeanton, H., Travi, Y., Blavoux, B., 2001. Isotopic typology of the precipitation in the Western Mediterranean region at three different time scales. Geophysical Research Letters 28(7), 1215-1218.

Chen, F.-H., Yu, Z., Yang, M., Ito, E., Wang, S., Madsen, D.B., Huang, X., Zhao, Y., Sato, T., Birks, H.J.B., Boomer, I., Chen, J., An, C., Wünnemann, B., 2008. Holocene moisture evolution in arid central Asia and its out-of-phase relationship with Asian monsoon history. Quaternary Science Reviews 27, 351–364.

Christophoul, F., Soula, J.-C., Brusset, S., Elibana, B., Roddaz, M., Bessiere, G., Deramond, J., 2003. Time, place and mode of propagation of foreland basin systems as recorded by the sedimentary fill: examples of the Late Cretaceous and Eocene retro-foreland basins of the north-eastern Pyrenees. Geological Society, London, Special Publications 208, 229-252, doi:10.1144/GSL.SP.2003.208.01.11.

Dansgaard, W., 1964. Stable isotopes in precipitation. Tellus 16, 436-468.

Ehlers, T.A., Poulsen, C.J., 2009. Influence of Andean uplift on climate and paleoaltimetry estimates. Earth and Planetary Science Letters 281 (3–4), 238–248.

Epstein, S., Mayeda, T., 1953. Variation of $^{18}O$ content of waters from natural sources. Geochimica et Cosmochimica Acta 4, 213-224.

Filleaudeau, P.Y., Mouthereau, F., Pik, R, 2012. Thermo-tectonic evolution of the south-central Pyrenees from rifting to orogeny: insights from detrital zircon U/Pb and (U-Th)/He thermochronometry. Basin Research 24, 401-417.

Fons, M.C., 1979. Cyclogenèses du bassin méditerranéen occidental. Monographie n°109, Météorologie Nationale.

Froehlich, K., Gibson, J. J., Aggarwal, P., 2001. Deuterium excess in precipitation and its climatological significance. In Study of Environmental Change Using Isotope Techniques. International Atomic Energy Agency, C&S Papers Series, 13, 54-66.

Garcia-Castellanos, D., Vergés, J., Gaspar-Escribano, J., Cloetingh, S., 2003. Interplay between tectonics, climate, and fluvial transport during the Cenozoic evolution of the Ebro Basin (NE Iberia). Journal of Geophysical Research 108 (B7), 2347, http://dx.doi. org/10.1029/2002JB002073.

Garzione, C.N., Quade, J., DeCelles, P.G., English, N.B., 2000. Predicting paleoelevation of Tibet and the Himalaya from $\delta^{18}O$ vs. altitude gradients in meteoric water across the Nepal Himalaya. Earth and Planetary Science Letters 183, 215–229.

Garzione, C.N., Auerbach, D.J., Smith, J.J.S., Rosario, J.J., Passey, B.H., Jordan, T.E., Eiler, J.M., 2014. Clumped isotope evidence for diachronous surface cooling of the Altiplano and pulsed surface uplift of the Central Andes. Earth and Planetary Science Letters 393, 173-181.

Gébelin, A., Mulch, A., Teyssier, C., Jessup, M.J., Law, R.D., Brunel, M., 2013. The Miocene elevation of Mount Everest. Geology 41, 799-802.

Gonfiantini, R., Roche, M.A., Olivry, J.C., Fontes, J.C., Zuppi, G.M., 2001. The altitude effect on the isotopic composition of tropical rains. Chemical Geololgy 181, 147–167.

Gunnell, Y., Zeyen, H., Calvet, M., 2008. Geophysical evidence of a missing lithospheric root beneath the eastern Pyrenees: consequences for post-orogenic uplift and associated geomorphic signatures. Earth and Planetary Science Letters 276, 302–313.

Hijmans, R., Cameron, S.E., Parra, J.L., Jones, P.G., Jarvis, A., 2005. Very high resolution interpolated climate surfaces for global land areas. International Journal of Climatology 25, 1965-1978

Huyghe, D., Mouthereau, F., Castelltort, S., Filleaudeau, P-Y., Emmanuel, L., 2009. Paleogene propagation of the southern Pyrenean thrust wedge revealed by finite strain analysis in frontal thrust sheets: implications for mountain building, Earth and Planetary Science Letters 288, 421-433.

Huyghe, D., Mouthereau, F., Emmanuel, L., 2012a. Oxygen isotopes of marine mollusc shells record Eocene elevation change in the Pyrenees. Earth and Planetary Science Letters 345-348, 131-141.

Huyghe, D., Castelltort, S., Mouthereau, F., Serra-Kiel, J., Filleaudeau, P.-Y., Berthier, B., Emmanuel, L., Renard, M., 2012b. Large scale facies change in the middle Eocene South-Pyrenean foreland basin: The role of tectonics and prelude to Cenozoic ice-age. Sedimentary Geology 253-254, 25-46.

IAEA/WMO, 2017. Global Network of Isotopes in Precipitation. The GNIP Database. Accessible at: http://www.iaea.org/water

Ingraham, N.L., Taylor, B.E., 1991. Light stable isotope systematics of large-scale hydrologic regimes in California and Nevada. Water Resources Research 27, 77–90.

Insel, N., Poulsen, C.J., Ehlers, T.A., Sturn, C., 2012. Response of meteoric $\delta^{18}O$ to surface uplift – Implications for Cenozoic Andean Plateau growth. Earth and Planetary Science Letters 317-318, 262-272.

Lambs, L., Moussa, I., Brunet, F., 2013. Air masses origin and isotopic tracers: a study case of the oceanic and Mediterranean rainfall southwest of France. Water 5, 617-628. doi: 10.3390/w5020617.

Lee, J.E., Fung, I., 2008. "Amount effect" of water isotopes and quantitative analysis of post- condensation processes. Hydrological Processes 22(1), 1-8.

Li, L., Garzione, C.N., 2017. Spatial distribution and controlling factors of stable isotopes in meteoric waters on the Tibetan Plateau: Implications for paleoelevation reconstruction. Earth and Planetary Science Letters 460, 302-314.

Longinelli, A., Selmo, E., 2003. Isotopic composition of precipitation in Italy: a first overall map. Journal of Hydrology 270, 75–88.

Merlivat L., Jouzel J., 1979. Global climatic interpretation of the deuterium-oxygen 18 relationship for precipitation. Journal of Geophysical Research 84 (C8), 5029-5033.

Morrison, J., Brockwell, T., Merren, T., Fourel, F., Phillips, A.M., 2001. On-Line High-Precision Stable Hydrogen Isotopic Analyses on Nanoliter Water Samples. Analytical Chemistry 73(15), 3570-3575.

Mouthereau, F., Filleaudeau, P.-Y., Vacherat, A., Pik, R., Lacombe, O., Fellin, M.G., Castelltort, S., Christophoul, F., Masini, E., 2014. Placing limits to shortening evolution in the Pyrenees: Role of margin architecture and implications for the Iberia/Europe convergence. Tectonics 33, doi:10.1002/2014TC003663.

Mulch, A., 2016. Stable isotope paleoaltimetry and the evolution of landscapes and life. Earth and Planetary Science Letters 433, 180-191.

Muñoz, J.A.E., 1992. Evolution of a continental collision belt: ECORS-Pyrenees crustal balanced cross-section, in: K. McClay, (Ed), Thrust Tectonics, Chapman & Hall, pp. 235-246.

Poage, M.A., Chamberlain, P., 2001. Empirical relationships between elevation and the stable isotope composition of precipitation and surface waters: considerations for studies of paleoelevation change. American Journal of Science 301, 1-15.

Quade, J., Breecker, D.O., Daëron, M., Eiler, J., 2011. The paleoaltimetry of Tibet: an isotopic perspective. American Journal of Science 311, 77-115.

Rowley, D.B., Currie, B.S., 2006. Paleo-altimetry of the late Eocene to Miocene Lunpola basin, central Tibet. Nature 439, 677–681.

Rowley, D.B., Garzione, C., 2007. Stable-isotope based paleoaltimetry. Annual Review of Earth and Planetary Science 35, 463–506.

Rowley, D.B., Pierrehumbert, R.T., Currie, B.S., 2001. A new approach to stable isotope-based paleoaltimetry: implications for paleoaltimetry and paleohypsometry of the High Himalaya since the Late Miocene. Earth of Planetary Science Letters 188, 253–268.

Schemmel, F., Mikes, T., Rojay, B., Mulch, A., 2013. The impact of topography on isotopes in precipitation across the Central Anatolian Plateau (Turkey). American Journal of Science 313, 61–80.

Schotterer, U., Frohlich, K., Gaggeler, H.W., Sandjordj, S., Stichler, W., 1997. Isotope records from Mongolian and alpine ice cores as climate indicators. Climatic Change 36, 519–530.

Sinclair, H.D., Gibson, M., Naylor, M., Morris, G., 2005. Asymetric growth of the Pyrenees revealed through measurement and modeling of orogenic fluxes. American Journal of Science 305, 369-406.

Stein, A.F., Draxler, R.R, Rolph, G.D., Stunder, B.J.B., Cohen, M.D., Ngan, F., 2015. NOAA's HYSPLIT atmospheric transport and dispersion modeling system, Bulletin of the American Meteorological Society 96, 2059-2077, http://dx.doi.org/10.1175/BAMS-D-14-00110.1.

Suc, J.-P., Fauquette, S., 2012. The use of pollen floras as a tool to estimate palaeoaltitude of mountains: The eastern Pyrenees in the Late Neogene, a case study. Palaeogeography, Palaeoclimatology, Palaeoecology 321-322, 41-54.

Vacherat, A., Mouthereau, F., Pik, R., Huyghe, D., Paquette, J.-L., Christophoul, F., Loget, N., Tibari, B., 2017 Rift-to-collision sediment routing in the Pyrenees: a synthesis from sedimentological, geochronological and kinematic constraints. Earth-Science Reviews 172, 43-74.

Vergés, J., Fernandez, M., Martinez, A., 2002. The Pyrenean orogen: pre-, syn-, and post-collisional evolution. In: Rosenbaum, G. and Lister, G. S. 2002. Reconstruction of the evolution of the Alpine-Himalayan Orogen. Journal of the Virtual Explorer 8, 55 - 74.

Winnick, M.J., Welker, J.M., Chamberlain, C.P., 2014. Quantifying the isotopic "Continental Effect". Earth and Planetary Science Letters 406, 123–133.

Figure-1

Click here to download Figure: Fig-1-carte ech-small.pdf

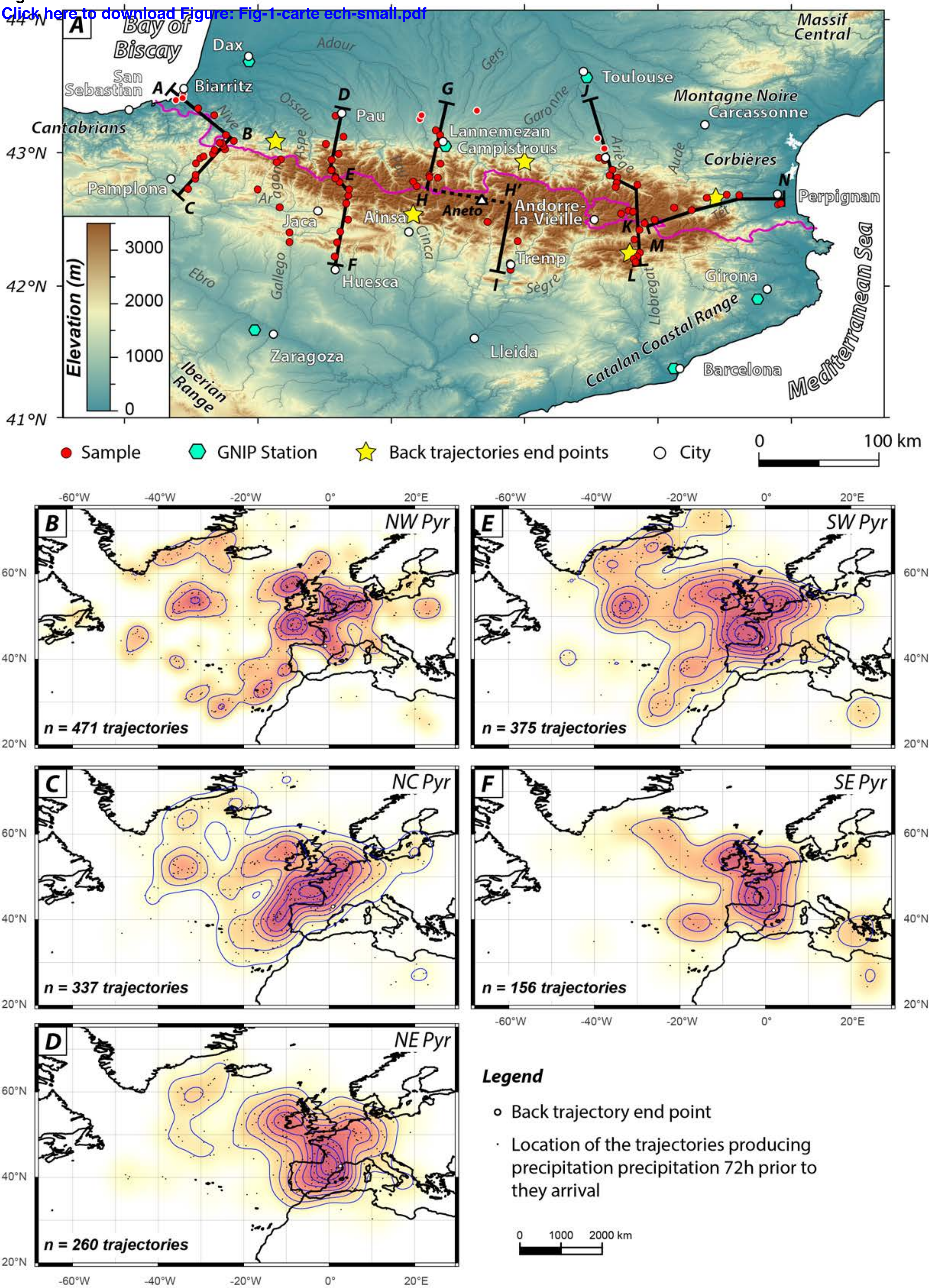

Figure-2
Click here to download Figure: Fig-2 MAT MAP V2-small.pdf

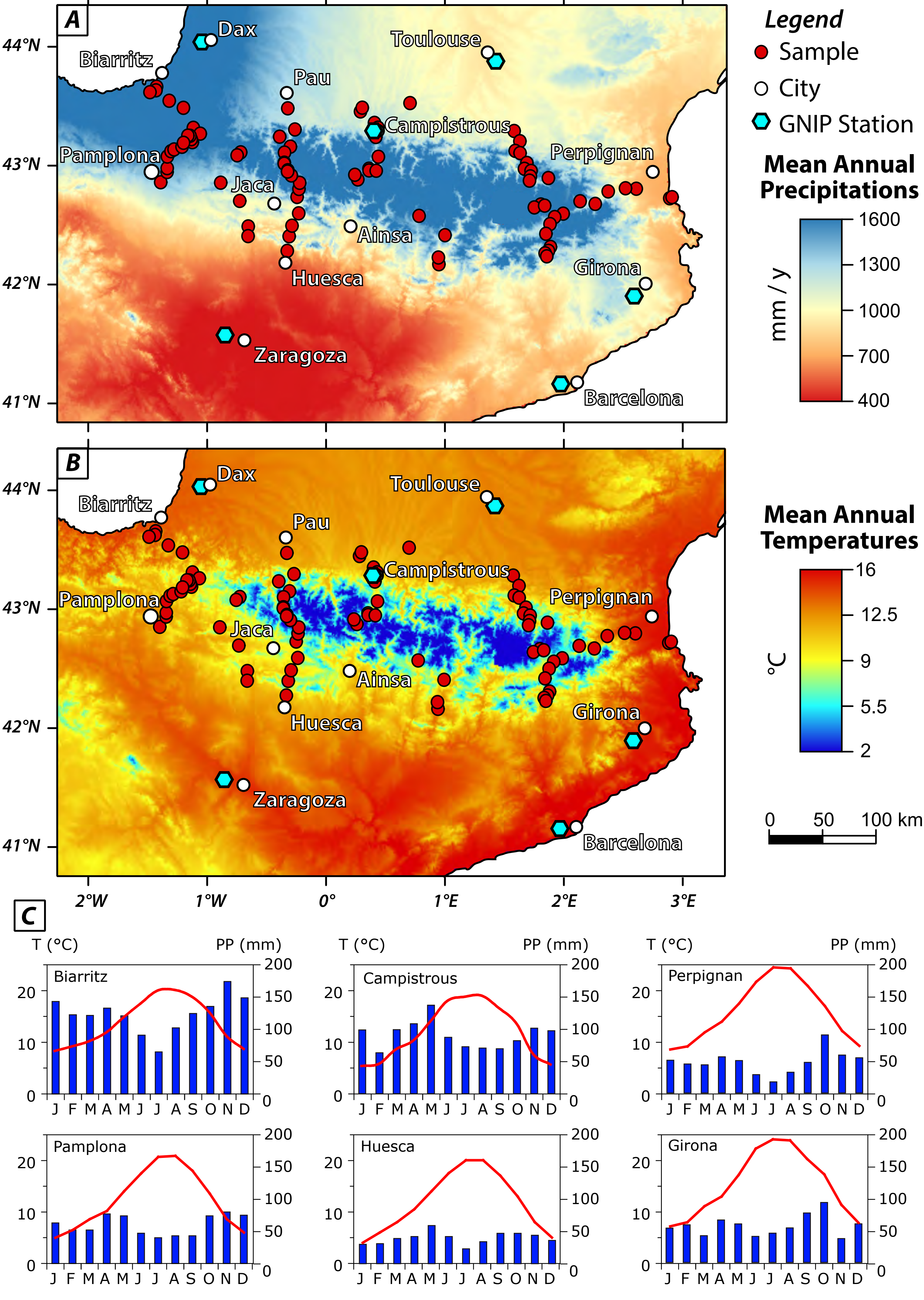

Figure-3

Click here to download Figure: Fig-3-d18O dD-small.pdf

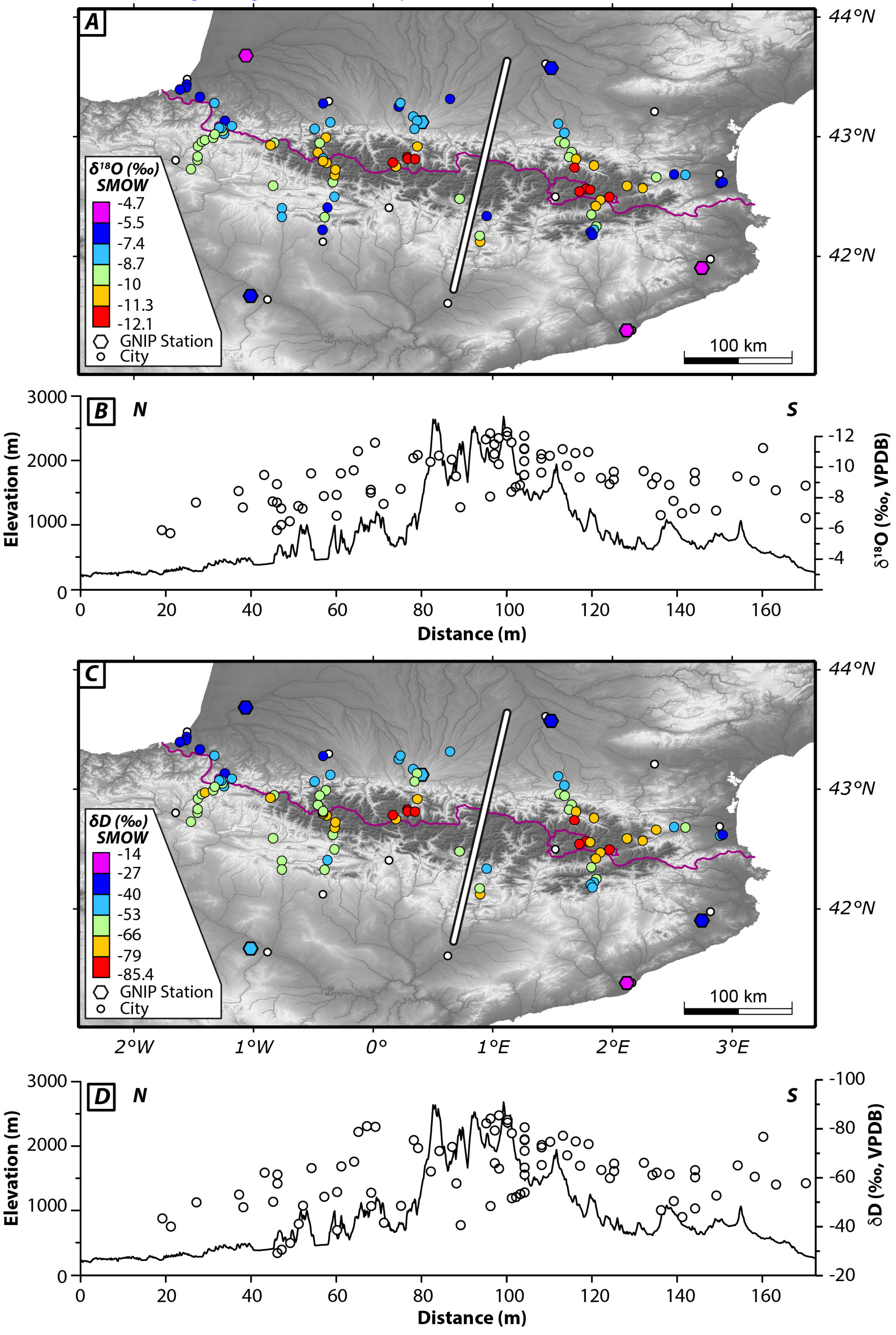

Figure-4

Click here to download Figure: Fig-4-profilsd18O.pdf

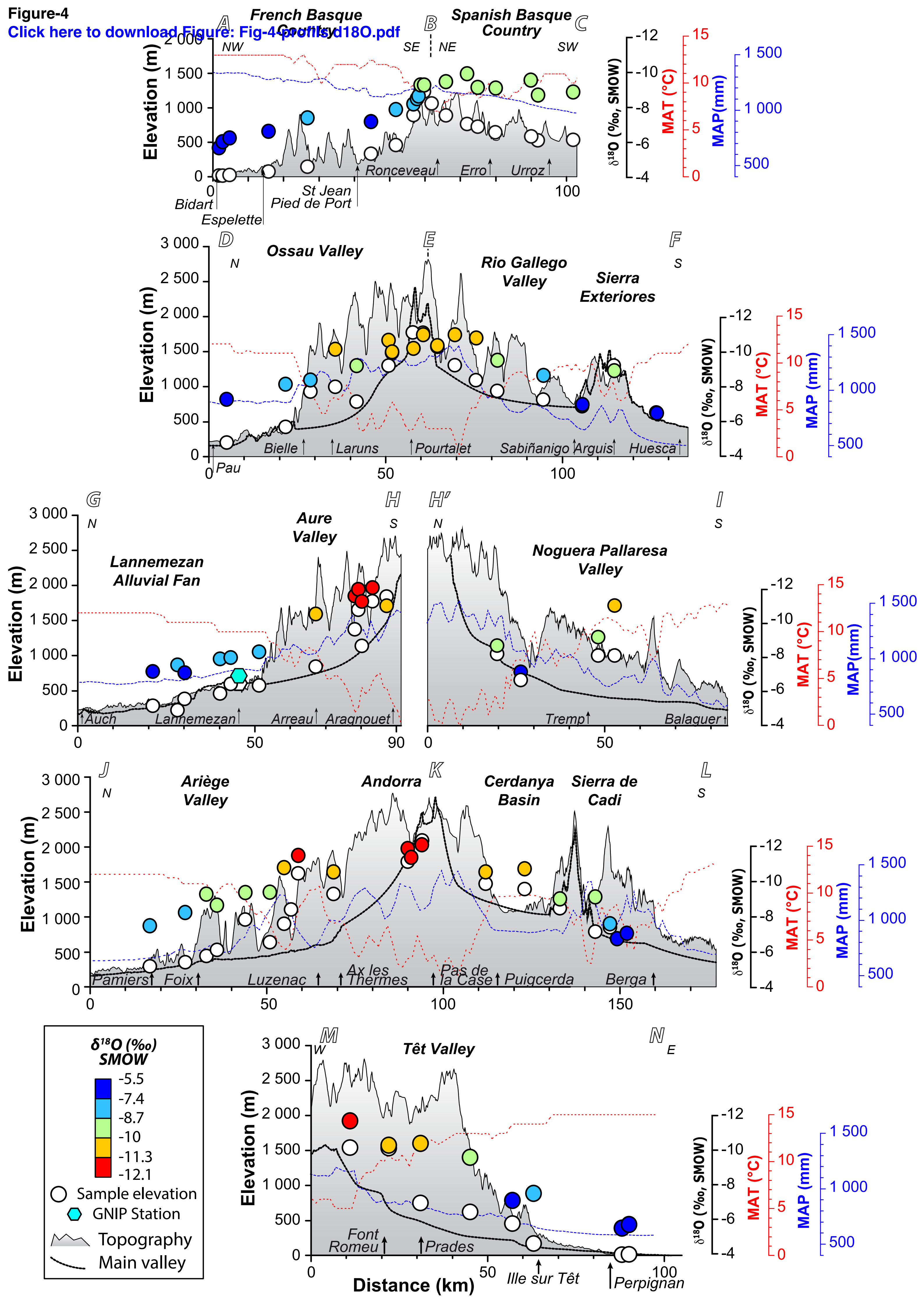

Figure-5

Click here to download Figure: Fig-5-profilsdD.pdf

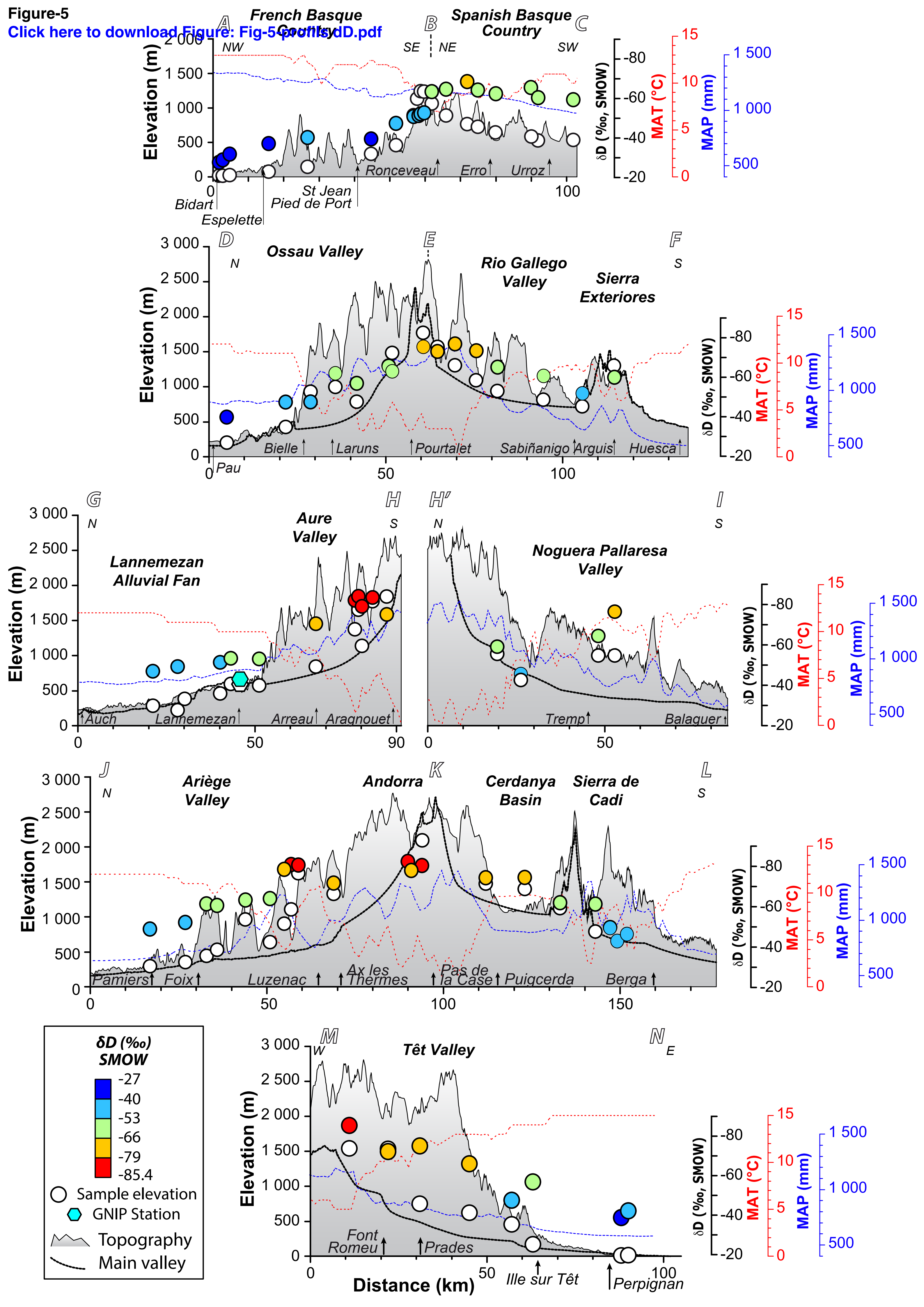

Figure-6

Click here to download Figure: Fig-6-d excess-small.pdf

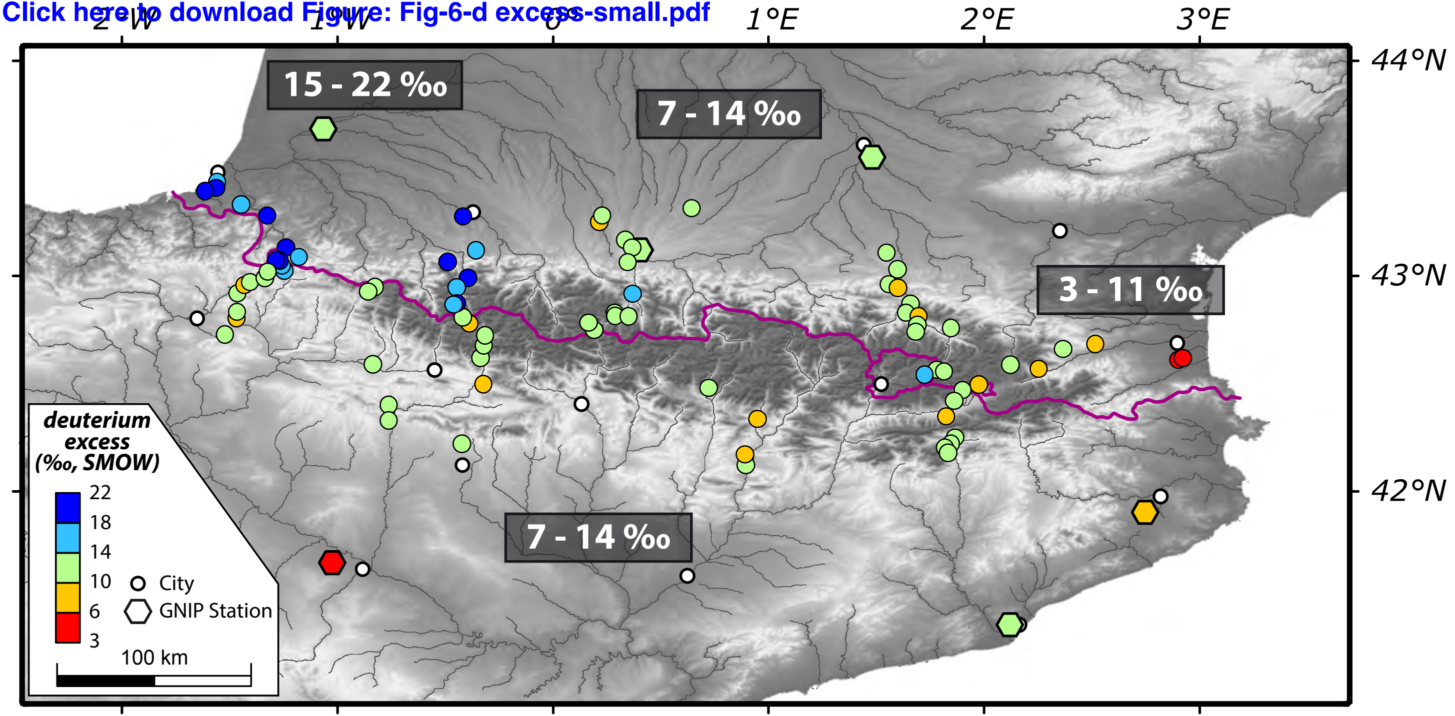

Figure-7
Click here to download Figure: Fig-7-d18O dD rivers-GNIP.pdf

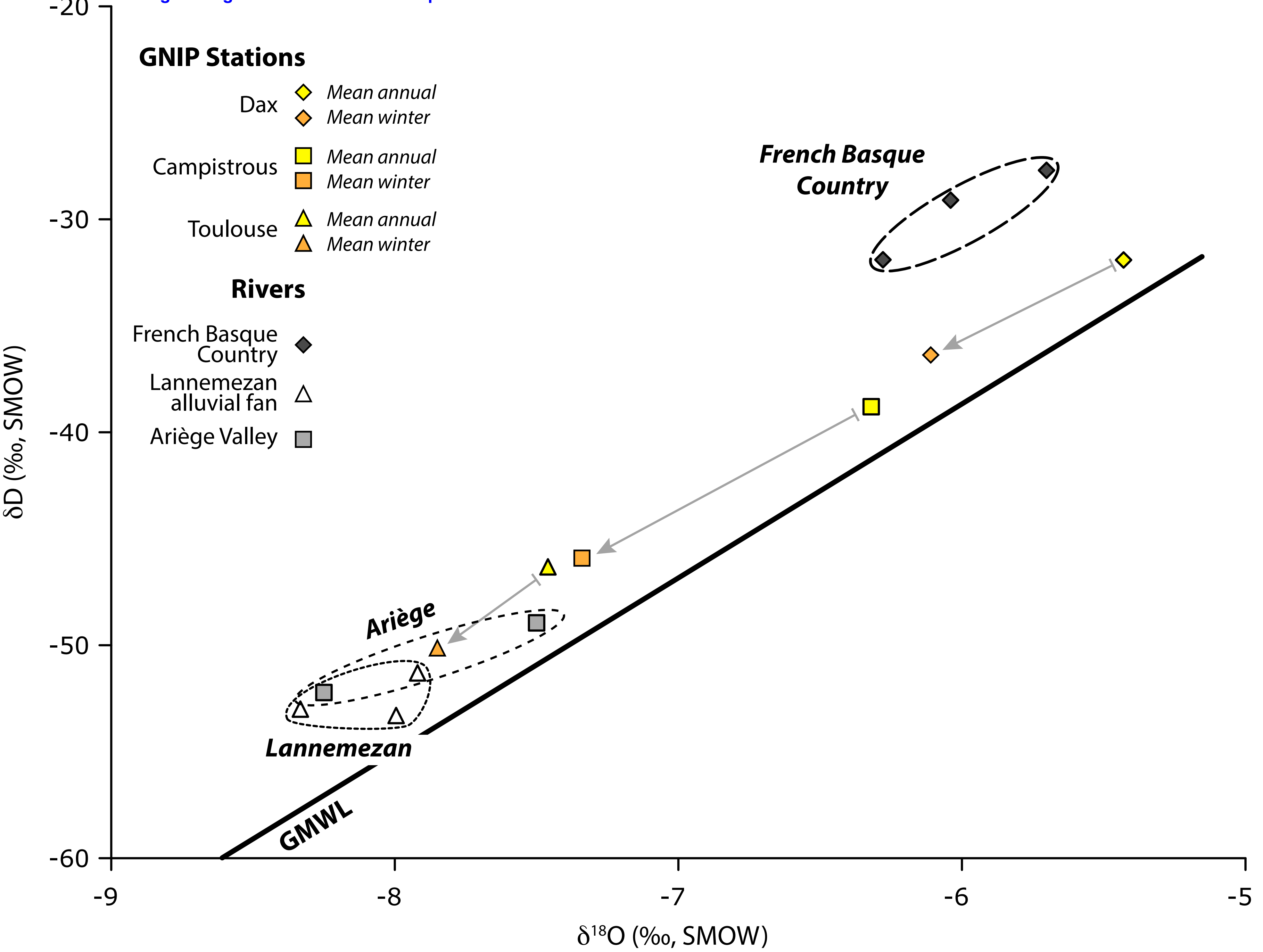

**Figure-8**

**Click here to download Figure: Fig-8 V2.pdf**

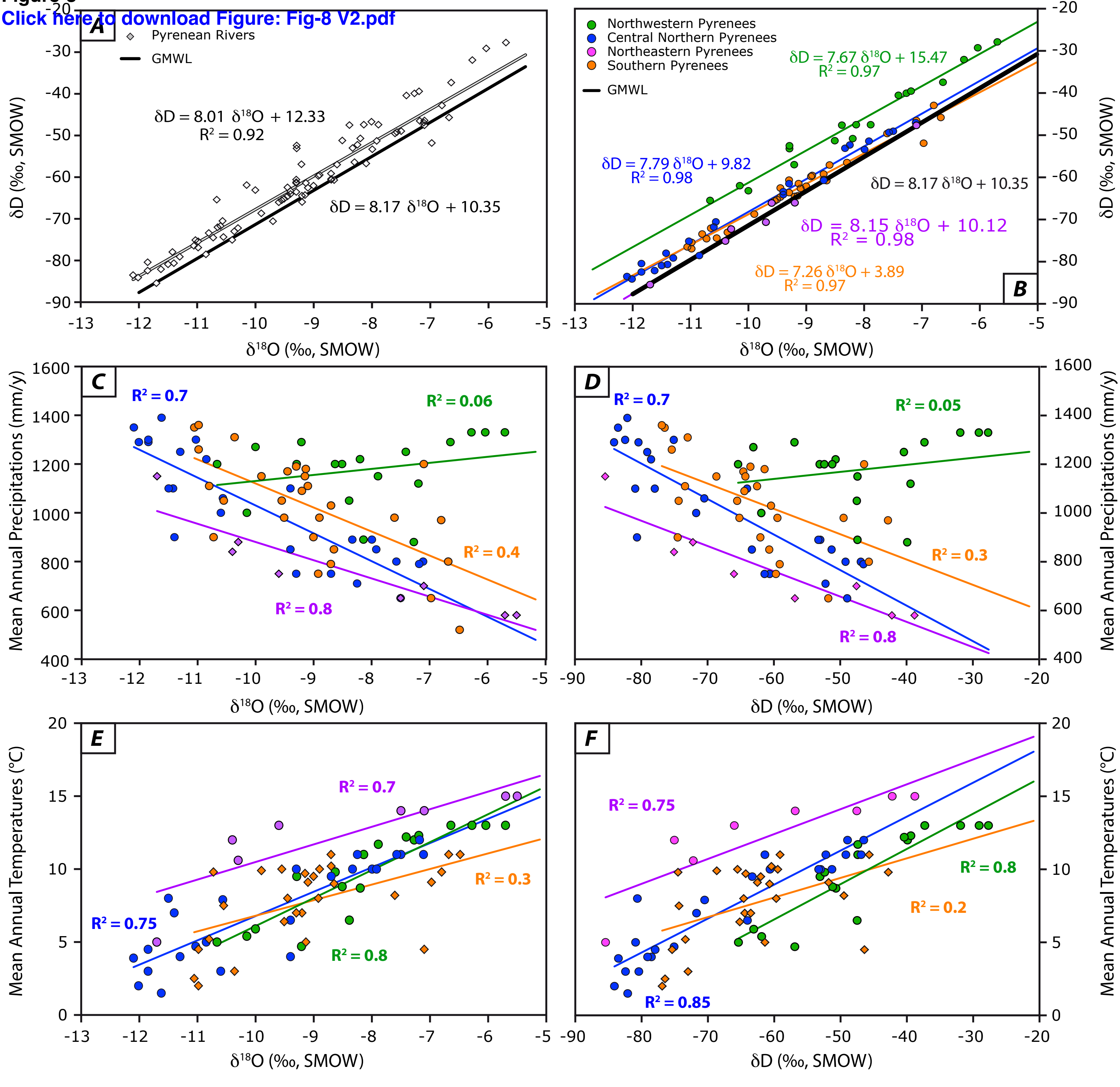

Figure-9

Click here to download Figure: Fig-9-d18O-Alt-Pyr.pdf

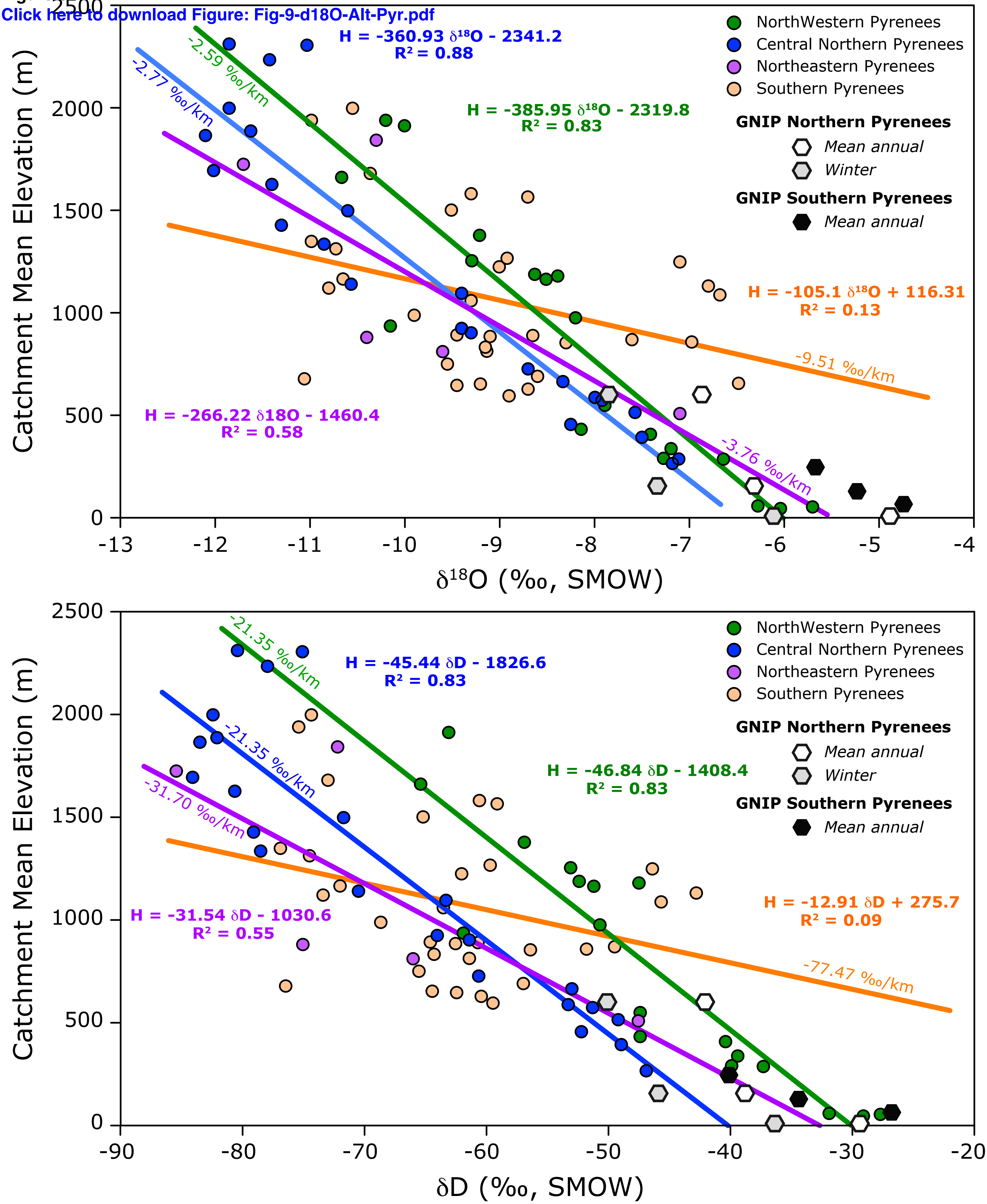

Figure-10
Click here to download Figure: Fig-10-d18O-Alt-Synthse.pdf